Algebraic Connectivity of Interdependent Networks

J. Martín-Hernández[a,*], H. Wang[a], P. Van Mieghem[a], G. D'Agostino[b]

[a] *Faculty of Electrical Engineering, Mathematics and Computer Science P.O Box 5031, 2600 GA Delft, The Netherlands*
[b] *ENEA Centro Ricerche Casaccia, via Anguillarese 301, I-00123 Roma (RM) , Italy*

Abstract

The algebraic connectivity μ_{N-1}, i.e. the second smallest eigenvalue of the Laplacian matrix, plays a crucial role in dynamic phenomena such as diffusion processes, synchronization stability, and network robustness. In this work we study the algebraic connectivity in the general context of interdependent networks, or network-of-networks (NoN). The present work shows, both analytically and numerically, how the algebraic connectivity of NoNs experiences a transition. The transition is characterized by a saturation of the algebraic connectivity upon the addition of sufficient coupling links (between the two individual networks of a NoN). In practical terms, this shows that NoN topologies require only a fraction of coupling links in order to achieve optimal diffusivity. Furthermore, we observe a footprint of the transition on the properties of Fiedler's spectral bisection.

Keywords: Network of Networks, Synchronization, Laplacian, Spectral Properties, System of Systems

1. Introduction

In the last decades, there has been a significant advance in understanding the structure and functioning of complex networks [1, 2]. Statistical models of networks are now widely used to describe a broad range of complex systems, from networks of human contacts to interactions amongst proteins. In particular, emerging phenomena of a population of dynamically interacting units has always fascinated scientists. Dynamic phenomena are ubiquitous in nature and play a key role within various contexts in sociology [3], and technology [4]. To date, the problem of how the structural properties of a network influences the convergence and stability of its synchronized states has been extensively investigated and discussed, both numerically and theoretically [5, 6, 7, 8, 9], with special attention given to networks of coupled oscillators [10, 11, 12, 13].

*Corresponding author
Email addresses: j.martinhernandez@tudelft.nl (J. Martín-Hernández), h.wang@tudelft.nl (H. Wang), p.f.a.vanmieghem@tudelft.nl (P. Van Mieghem), gregorio.dagostino@enea.it (G. D'Agostino)

In the present work, we focus on the second smallest eigenvalue μ_{N-1} of a graph's Laplacian matrix, also called *algebraic connectivity*. This metric plays an important role on, among others, synchronization of coupled oscillators, network robustness, consensus problems, belief propagation, graph partitioning, and distributed filtering in sensor networks [14, 15, 16, 17, 18]. For example, the time it takes to synchronize Kuramoto oscillators upon any network scales with the inverse of μ_{N-1} [19, 20, 21, 22]. In other words, larger values of μ_{N-1} enable synchronization in both discrete and continuous-time systems, even in the presence of transmission delays [23, 24]. As a second application, graphs with "small" algebraic connectivity have a relatively clean bisection, i.e. the smaller μ_{N-1}, the fewer links must be removed to generate a bipartition [25]. Furthermore, we illustrate the role of the algebraic connectivity in the diffusion dynamic process. For the sake of simplicity, we model the diffusive dynamics as a commodity exchange governed by the following differential equation:

$$\frac{ds_i}{dt} \approx \sum_{j \in N_i} (s_i(t) - s_j(t)) \approx \sum\nolimits_{j=1}^{N} Q_{ij} s_j(t); \tag{1}$$

where s_i represents the commodity or the state of the $i-th$ component, N_i its neighbors, and Q the Laplacian matrix, as further defined in section 2. The equilibrium state is that in which all gradients in (1) reach zero, thus the rate of the slowest exponential decay (of the deviation from the equilibrium) is proportional to the algebraic connectivity [26]. Hence, the higher the algebraic connectivity of the Q matrix, the smaller the "proper time".

Despite the latest advances in the research on synchronization and graph spectra, current research methods mostly focus on individual networks treated as isolated systems. In reality, complex systems are seldom isolated. For example, a power grid and a communication network may strongly depend on each other. A power station depends on a communication node for information, whereas a communication node depends on a power station for electricity [20]; similarly, a pathogen may spread from one species to another. Much effort has been devoted to predict cascading effects in such interdependent networks [27, 28, 29]: the largest connected component has been shown to exhibit a spectacular phase transition after a critical number of faults is reached. Quite recently, a novel approach has been introduced by resorting to the spectral analysis of interdependent networks. By means of the graph spectra, the epidemic thresholds of interdependent networks have been estimated, and absolute boundaries have been provided [27]. These scenarios motivated us to study the influence of interdependent networks on diffusive processes via their spectral properties.

In this work, we show analytically and numerically how the algebraic connectivity of interdependent networks experiences a phase transition upon the addition (or removal) of a sufficient number of interlinks between two identical networks. As a direct consequence, the proper time of a diffusion process on top of the NoN system is not affected by interlink additions, as long as the number of interlinks is higher than a critical threshold. The location of the described transition depends on the link addition strategy, as well as on the algebraic connectivity of the single networks. Gomez *et al.* [30] applied perturbation theory to approximate lower bounds for μ_{N-1} in a multiplex scenario, for which they conclude that

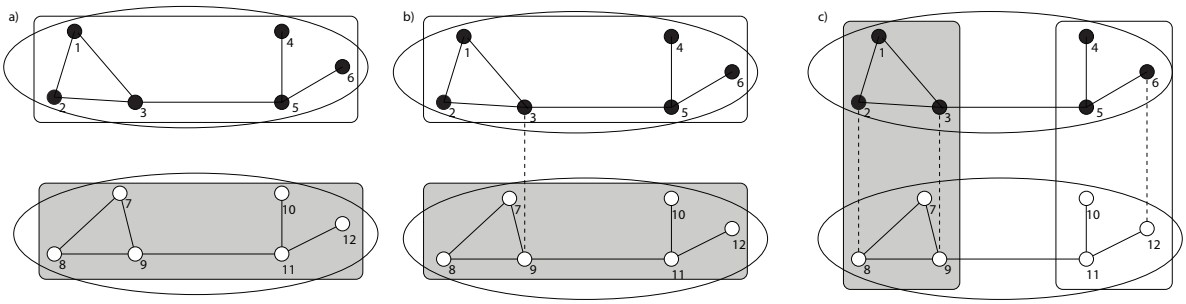

Figure 1: Two graphs, with 6 nodes, and 7 links each (solid lines) are subject to spectral partitioning based on the Fiedler vector, i.e. the eigenvector corresponding to the algebraic connectivity. The two single graphs are encircled with ovals, and the corresponding spectral partitioning is represented by rectangles. The single graphs are progressively coupled with *a)* no interlinks, *b)* 1 interlink and *c)* 3 interlinks (dashed lines). As we can see, adding 1 interlink causes the spectral partitioning algorithm to split the network into the two original partitions. Upon the addition of 3 or more interlinks, the spectral partition experiences a brusque transition, causing the single networks intralinks (solid lines) to become the new confining links.

interdependent networks speed up diffusion processes. Although the latter study hints the existence of a sudden shift, their authors over-sighted the existence of a phase transition, which we fully characterize via mean-field theory and by investigating additional spectral properties for different values of N. In particular, we observe that the phase transition is reflected in spectral partitioning algorithms, as illustrated in Figure 1.

This paper is structured as follows. Section 2 introduces some required terminology, the Laplacian matrix, and its corresponding spectra. Sections 3.1 and 3.2 provide some analytical results for the algebraic connectivity of interdependent networks, based on both mean-field approach and perturbation theory, respectively. Our models are able to predict the fraction of links that will cause the algebraic connectivity transition. Finally, Section 4 validates our previous results through extensive numerical results. This section also exposes results on regular, random, small-world, and scale-free networks. Conclusions are drawn in Section 5.

2. Definitions

2.1. Graph Theory Basics

A graph G is composed by a set of *nodes* interconnected by a set of *links* $G(\mathcal{N}, \mathcal{L})$. Suppose one has two networks $G_1 = (\mathcal{N}_1, \mathcal{L}_1)$ and $G_2 = (\mathcal{N}_2, \mathcal{L}_2)$, each with a set of nodes $(\mathcal{N}_1, \mathcal{N}_2)$ and a set of links $(\mathcal{L}_1, \mathcal{L}_2)$ respectively. For simplicity, in the following we will suppose any dependence relation to be symmetric, i.e. all networks are undirected.

The global system resulting from the connection of the two networks is a network G with $\mathcal{N}_1 \cup \mathcal{N}_2$ nodes and $\mathcal{L}_1 \cup \mathcal{L}_2$ "intralinks" plus a number of "interlinks" $\mathcal{L}_{12}$ joining the two networks; that is $\mathcal{N} = \mathcal{N}_1 \cup \mathcal{N}_2$ and $\mathcal{L} = \mathcal{L}_1 \cup \mathcal{L}_2 \cup \mathcal{L}_{12}$, thus $(\mathcal{N}, \mathcal{L}) = G \stackrel{def}{=} (\mathcal{N}_1 \cup \mathcal{N}_2, \mathcal{L}_1 \cup \mathcal{L}_2 \cup \mathcal{L}_{12})$.

Let us denote N_i as the number of nodes in $|\mathcal{N}_i|$, and L_i as the number of links in as $|\mathcal{L}_i|$, also $N = N_1 + N_2$, and $L = L_1 + L_2$; let A_1 and A_2 be the adjacency matrices of the

two networks G_1 and G_2, and A that of the whole system G, whose entries or elements are $a_{ij} = 1$ if node i is connected to node j, otherwise $a_{ij} = 0$. When the two networks are disconnected ($\mathcal{L}_{12} = \emptyset$), the matrix A is defined as the $N \times N$ matrix:

$$A = \begin{bmatrix} A_1 & \mathbf{0} \\ \mathbf{0} & A_2 \end{bmatrix}.$$

When an interaction is introduced ($\mathcal{L}_{12} \neq \emptyset$), the adjacency matrix acquires non-trivial off-block terms denoted by B_{ij}, defined as the $N_i \times N_j$ interconnection matrix representing the *interlinks* between G_1 and G_2. The interdependency matrix B is then

$$B = \begin{bmatrix} \mathbf{0} & B_{12} \\ B_{12}^T & \mathbf{0} \end{bmatrix}.$$

and adjacency matrix of the total system can be written as:

$$A + \alpha B = \begin{bmatrix} A_1 & \alpha B_{12} \\ \alpha B_{12}^T & A_2 \end{bmatrix}. \tag{2}$$

where α represents the coupling strength of the interaction.

Similarly to the adjacency matrix, one may introduce the Laplacian matrix $Q = D - A$; where D is the diagonal matrix of the degrees, where the degree of the i-th node is $d_i \stackrel{def}{=} \sum_j a_{ij}$. In the same vein, one may define the diagonal matrices:

$$\begin{cases} (D_1)_{ii} & \stackrel{def}{=} & \sum_j (B_{12})_{ij}, \\ (D_2)_{ii} & \stackrel{def}{=} & \sum_j (B_{21})_{ij} = \sum_j (B_{12}^T)_{ij}; \end{cases}.$$

and the Laplacian Q of the total system G reads:

$$Q = Q_A + \alpha Q_B = \begin{bmatrix} Q_1 + \alpha D_1 & -\alpha B_{12} \\ -\alpha B_{12}^T & Q_2 + \alpha D_2 \end{bmatrix}. \tag{3}$$

where $Q_1 = Q_2$ is the Laplacian matrix of $A_1 = A_2$, and Q_B is the Laplacian only representing the interlinks:

$$Q_B = D - B = \begin{bmatrix} D_1 & -B_{12} \\ -B_{12}^T & D_2 \end{bmatrix}. \tag{4}$$

2.2. Fiedler Partitioning

A graph bipartition is defined as two disjoint sets of nodes $\{\mathcal{R}, \mathcal{S}\}$, where $\mathcal{R} \cup \mathcal{S} = \mathcal{N}$. In addition, we define the *natural partition* of G as the bipartition that coincides with the two original node sets: $\mathcal{R} = \mathcal{N}_1$, and $\mathcal{S} = \mathcal{N}_2$, as illustrated in Fig. 2. The number of nodes in $\mathcal{R}$ and $\mathcal{S}$ is counted by their cardinality $|\mathcal{R}|$ and $|\mathcal{S}|$, respectively.

Since Q is a non-negative real symmetric matrix, it has N real eigenvalues [26], which we order non-decreasingly $0 = \mu_N \leq \mu_{N-1} \leq \cdots \leq \mu_1$. The eigenvector x_{N-1} corresponding to the first non-zero eigenvalue μ_{N-1} provides a spectral bipartition named after Fiedler, who

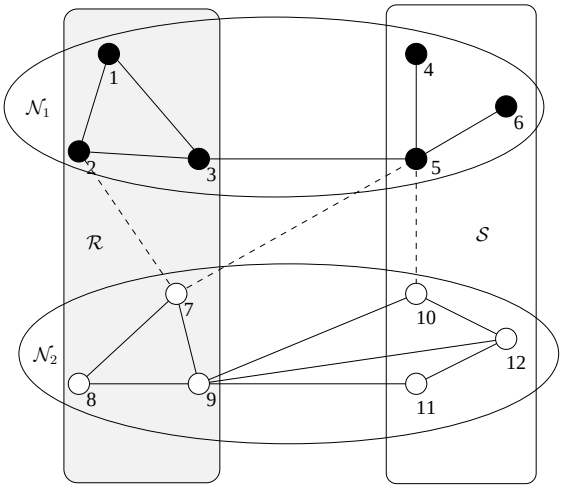

Figure 2: The four main partition sets are displayed: $\mathcal{N}_1$ (set of black nodes), $\mathcal{N}_2$ (set of white nodes), $\mathcal{R}$ (set of nodes within the gray rectangle), and $\mathcal{S}$ (set of nodes within the white rectangle). Both, the partition sets and the interlinks (dashed lines) were arbitrary chosen for illustration purposes and do not represent the corresponding Fiedler partition.

derived the majority of its properties [17, 31]. Since this paper only deals with the Fiedler eigenvector, we will simplify the notation of the eigenpair (μ_{N-1}, x_{N-1}) by simply writing (μ, x). Fiedler partitioning bisects the nodes of $\mathcal{N}$ into two clusters, such that two nodes i and j belong to the same cluster if $x_i x_j > 0$, i.e. the corresponding components of the Fiedler eigenvector x have the same sign. For example, if the coupling strength α in (3) is zero, the bipartition resulting from Fiedler partitioning is equivalent to the two natural clusters, i.e. $\mathcal{R} = G_1$ and $\mathcal{S} = G_2$.

In order to quantify the effect of the Fiedler partition on interdependent networks, we will study the three following spectral partitioning metrics:

- *Fiedler cut-size* $\stackrel{def}{=} \frac{l(\mathcal{R},\mathcal{S})}{L_1+L_2}$, where $l(\mathcal{R},\mathcal{S}) = l(\mathcal{S},\mathcal{R})$ equals the number of links with one end node in $\mathcal{R}$ another end node in $\mathcal{S}$. The Fiedler cut-size represents the fraction of links with one end in $\mathcal{R}$ and another end in $\mathcal{S}$ (irrespective of the directionality of the link) over the starting number of links.

- *interdependence angle*, defined as the angle between the normalized Fielder vector x and the versor $x^{(0)} = \frac{1}{\sqrt{N}}(1, \ldots, 1, -1, \ldots, -1)$, which we explain in detail in Appendix A. The interdependence angle is minimized when the Fiedler vector is parallel to $x^{(0)}$, i.e. when the Fiedler partition matches the natural partition.

- *entropy* H of the squared Fiedler vector components $H \stackrel{def}{=} -\sum_{i=1}^{N} {x_i}^2 \log {x_i}^2$. Based on Shannon's information theory metric, the entropy indicates how homogeneous the values in x are, similarly to the participation ratio or vector localization. The higher the entropy, the lower the dispersion among the values in x.

Some partition quality metrics may be undefined if the Laplacian matrix Q is defective [32]. In particular, if the second and third smallest eigenvalues of $Q_A + \alpha Q_B$ are equal $\mu_{N-1} = \mu_{N-2}$ then any linear combination $x' = ax_{N-1} + bx_{N-2}$ is also an eigenvector of Q with eigenvalue μ_{N-1}, thus the Fiedler vector is not uniquely defined. However we will ignore these cases, which tend to occur only in graphs with deterministic structures (e.g. the cycle graph [26]).

3. Analytical Results

This section introduces two independent analytical approaches to compute μ for the interdependent graph setup described in the previous section. The two approaches are based on mean-field theory and perturbation theory, which span Section 3.1 and Section 3.2, respectively. For a small number of added interlinks, both of the proposed theories are in agreement with each other, which validates our analysis.

3.1. Exact results for mean-field theory

3.1.1. Diagonal interlinking

Let us start with the case of two identical networks connected by $\mathcal{L}_{12}$ corresponding interlinks, which we refer to as "diagonal interlinking". We can add as little as 1 link and as many as N links. This strategy was chosen to achieve the maximum effect by meticulously adding a small number of interlinks.

The mean-field approach to such a system consists in studying a graph of two identical networks interacting via N_1 weighted connections among all corresponding nodes. The weight of each link, represented by $\alpha = \frac{L_{12}}{N_1}$, equals the fraction of nodes linked to their corresponding neighbour in the exact network. In other words $B_{12} = I$, such that the synchronization interdependence is modulated by the parameter α:

$$Q_A + \alpha Q_B = \begin{bmatrix} Q_1 + \alpha I & -\alpha I \\ -\alpha I & Q_2 + \alpha I \end{bmatrix}. \tag{5}$$

In the language of physics, α represents the coupling constant of the interaction between the networks. Consistently with the rest of the paper, this system will also be referred to as the mean-field model of the *diagonal interlinking* strategy. Regardless of its origin, this system exhibits some interesting properties worth discussing.

Let $\xi_{N_1}, \xi_{N_1-1}, ..., \xi_1$ be the set of eigenvectors for the Laplacian of the single network A_1, and $\omega_{N_1}, \omega_{N_1-1}, ..., \omega_1$ be their relative eigenvalues. Since the perturbation Q_B commutes with Q_A, all the eigenvectors of the interdependent graph are kept unchanged [26]. All the (unperturbed) eigenvalues are degenerate in pairs and, hence, one may define a set of eigenvectors based on those of the single networks:

$$\begin{cases} x_{2i} = \begin{bmatrix} \xi_i \\ \xi_i \end{bmatrix}. \\ x_{2i+1} = \begin{bmatrix} \xi_i \\ -\xi_i \end{bmatrix}. \end{cases} \tag{6}$$

The eigenvalues for the total non-interacting system (i.e. $\alpha = 0$) are the same as those of the unperturbed system $\mu_{2i} = \mu_{2i+1} = \omega_i$, hence, the ascending sequence of eigenvalues for the non-interactive system is $\omega_{N_1} = 0, 0, \omega_{N_1-1}, \omega_{N_1-1} \ldots, \omega_1, \omega_1$. When the interaction is switched on (i.e. $\alpha \neq 0$), assuming that $A_1 = A_2$, a trivial proof shows that the even eigenvalues are kept unaltered, while the odd ones increase linearly by the same amount 2α,

$$\begin{cases} \mu_{2i} = \omega_i, \\ \mu_{2i+1} = \omega_i + 2\alpha. \end{cases} \tag{7}$$

For α close to zero, the eigenvector ranking is kept unchanged $\mu_N = \omega_{N_1} = 0, \mu_{N-1} = 2\alpha, \mu_{N-2} = \omega_{N_1-1}, \mu_{N-3} = \omega_{N_1-1} + 2\alpha, \ldots, \omega_1, \omega_1 + 2\alpha$. However, when $\alpha > \frac{\omega_{N_1-1}}{2}$ the second and third smallest eigenvalues of the interdependent network (μ_{N-1} and μ_{N-2}) swap. Therefore, the first non-zero eigenvalue increases linearly with 2α up to the value of the isolated networks ω_{N_1-1} at which it reaches a plateau. In terms of equation (1), when α is greater than the threshold $\alpha_I = \frac{\omega_{N_1-1}}{2}$, the interactive system is capable of synchronizing with the same promptness as the single isolated network. Thus when the system coupling channel is quicker than the *proper time*, the time it takes the interactive system to reach equilibrium equals that of the single network. The critical value α_I for the exact model corresponds to a critical value of links l_I to be included to achieve the promptness of the single network:

$$l_I = \alpha_I N_1 = \frac{\omega_{N-1} \cdot N_1}{2}. \tag{8}$$

3.1.2. Random interlinking

As a variation of the localized diagonal interlinking, we have introduced a second strategy that may be treated algebraically; it corresponds to the mean field approximation of two identical networks interacting via L_{12} random connections, which we named *random interlinking* strategy.

The mean-field approach leads to an interdependence matrix with all unitary components: $B_{12} = J$, where J is the all ones matrix; the weight of each interlink is $\alpha = \frac{L_{12}}{N_1^2}$, and

$$Q = Q_A + \alpha Q_B = \begin{bmatrix} Q_1 + \alpha N_1 I & -\alpha J \\ -\alpha J & Q_2 + \alpha N_1 I \end{bmatrix}. \tag{9}$$

As in the previous case, the Q_B matrix commutes with Q_A, hence a common set of eigenvectors can be chosen (6). The null eigenvalue μ_N is always present, while all the others experience some increase for a non-trivial α: all eigenvalues μ_i for i smaller than $N-1$, increase for a fixed amount αN_1, while μ_{N-1} increases by twice that quantity,

$$\begin{cases} \mu_N & = 0, \\ \mu_{N-1} & = 2\alpha N_1, \\ \mu_i & = \omega_i + \alpha N_1, \text{ for } i \leq N-1. \end{cases} \tag{10}$$

This different rate of growth again implies that there exists a critical value α_J beyond which the second and third eigenvectors (μ_{N-1} and μ_{N-2}) swap. The threshold α_J can be obtained by imposing the crossing condition $\mu_{N-1} = \mu_{N-2}$,

$$\alpha_J = \frac{\omega_{N-1}}{N_1}. \tag{11}$$

Knowing that $\alpha = \frac{L_{12}}{N_1^2}$, we can estimate the critical number of links for the random interlinking strategy as

$$l_J = \alpha_J N_1^2 = \omega_{N-1} \cdot N_1. \tag{12}$$

It is worth noting that, the critical number of interlinks corresponding to the mean-field theory of the diagonal (8), and general (12) interlink strategies, differ simply by a factor of two.

3.1.3. Physical interpretation

If we interpret network robustness as the ability of a system to perform its function upon damage or attacks, then it is worth discussing what happens when two networks, A_1 and A_2, originally fully connected by diagonal interlinking B, are subject to some interlink loss or intentional attacks. Our simple, exact model shows that when these two fully connected networks are subject to minor interlink loss, the response of the total interacting system $A + \alpha B$ takes place at the same speed as the single component network A_1. In other words, when the operability of the control channel via α is mildly reduced, the global system synchronizability does not decrease. However if the operability of the connection devices degrades below the critical value α_I, the synchronization process starts to slow down. From the mean-field approach point of view, this means that the system may lose a fraction of interlinks while keeping its synchronization time unchanged.

Following the statistical perspective, the parameter α can be regarded as a coupling constant. If one identifies the Fiedler eigenvalue μ_{N-1} with the internal energy of a thermodynamical system, then its first derivative exhibits a jump from zero to a finite value. Nevertheless, this derivative does not diverge as expected for a second order[1] transition [33]. On the other hand, if one employs the Fiedler eigenvalue as a metric for the synchronizability and regards it as a thermodynamical potential such as the free enthalpy, its Legendre transform corresponds to the internal energy and exhibits a discontinuity at $\alpha = \alpha_I$. In this perspective, one may interpret the observed abrupt change as a first order phase transition. Despite this interesting parallel, it is worth noting that the Fiedler eigenvalue and its Legendre transform are not extensive quantities and, hence, they cannot be properly regarded as thermodynamical potentials. The question whether this abrupt change results from some hidden statistical artifact remains open.

To understand the intimate nature of the phase transition, one may inspect the topological properties of the eigenvectors. Below the critical value α_I, the cut links associated

[1]The order of a phase transition is the order of the lowest differential which shows a discontinuity.

to the Fiedler partition are localized outside the original networks (i.e. interlinks are cut), whereas just above the critical value, all cut links lay inside the originally isolated networks (i.e. intralinks are cut). This means that, below α_I, the synchronization is dominated by the intralinks in αB, while beyond α_I the synchronization involves the whole system, $A + \alpha B$.

3.2. Approximating μ using perturbation theory

In order to validate our mean-field analysis, we conducted a perturbative analysis of the Laplacian spectra. Perturbation theory provides insights on diffusion processes by analytically describing μ_{N-1} when the diffusive coupling between G_1 and G_2 is asymptotically small or large.

The problem consists in finding the minimum of the associated quadratic form in the unitary sphere ($x^T x = 1$), with the constraint $u^T x = 0$.

$$\mu = \mu_{N-1} = \inf_{x \neq 0, u^T x = 0} \frac{x^T Q x}{x^T x}; \tag{13}$$

In our case, the matrix Q is the sum of a matrix Q_A linking only nodes inside the same net, and a "perturbation" αQ_B that only connects nodes in different networks ($Q_A + \alpha Q_B$). Therefore, we want to find the minimum that satisfies the spectral equations:

$$\begin{cases} (Q_A + \alpha Q_B - \mu I)x &= 0, \\ x^T x &= 1, \\ u^T x &= 0. \end{cases} \tag{14}$$

When the solution is analytical in α, one may express μ and x by Taylor expansion as

$$\mu = \sum_{k=0}^{\infty} \mu^{(k)} \alpha^k \tag{15}$$

$$x = \sum_{k=0}^{\infty} x^{(k)} \alpha^k \tag{16}$$

Substituting the expansion in the eigenvalue equation (13) gives a hierarchy of equations. Solving the latter up to the second order yields the following approximations,

$$\mu^{(1)} = \left(x^{(0)}\right)^T Q_B x^{(0)} \tag{17}$$

$$\mu^{(2)} = \left(x^{(0)}\right)^T Q_B \left(x^{(1)}\right) = -\left(x^{(1)}\right)^T Q_A \left(x^{(1)}\right) \leq 0. \tag{18}$$

Appendix A describes the process used to reach the solution. As expected, the first order $\mu^{(1)}$ only depends on the zero order eigenvector $x^{(0)}$; the second order $\mu^{(2)}$ is negative thus improving the estimate of the algebraic connectivity. The former perturbation estimates are illustrated in Fig. 3 together with numerical simulations.

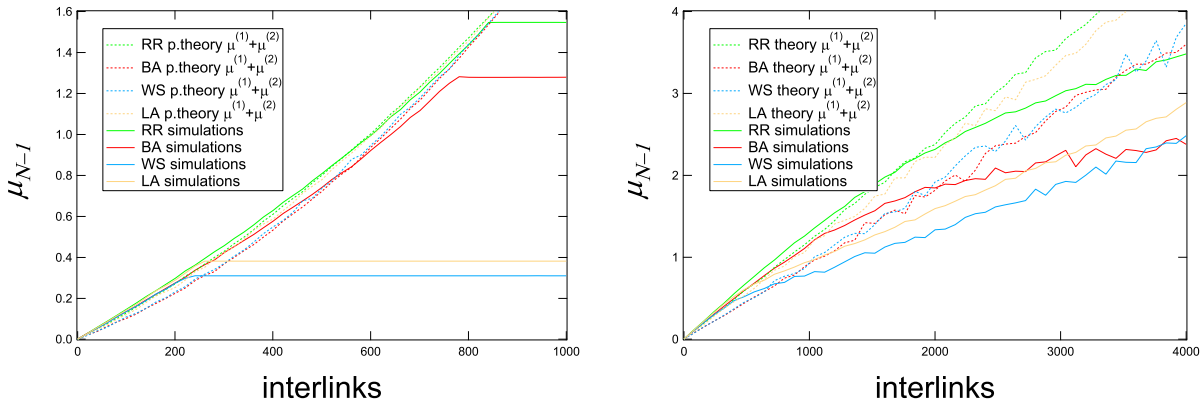

(a) Diagonal strategy

(b) Random strategy

Figure 3: Algebraic connectivity μ_{N-1} of four graph models with $N = 1000$ nodes, as simulated over different networks (solid lines) and approximated by second order perturbation theory (dashed lines). Interlinks are added between single networks following two strategies: diagonal interlinks (left image) and random interlinks (right image). Perturbation theory best approaches μ_{N-1} for the parabolic region of the diagonal interlinks strategy, which saturates after adding $\frac{\alpha_{Th} \cdot N}{2}$ links, as we detailed in section 3.1.

4. Simulations

The previous section provided two analytical means to estimate the dependence of μ_{N-1} on the topology of the interdependence links, namely mean field and perturbation theory. In this section we will introduce four model networks to test the predictability and the limits of our predictions.

4.1. Interdependent networks model

Our interdependent network model consists of two main components: a network model for the single networks, and the rules by which the two networks are linked as defined in Section 2. In other words, to model two interdependent networks one needs to select two model networks and one interlinking strategy.

In the numerical simulations discussed here, we considered four different graph models for our coupled networks:

- **Random Regular (RR)**: random configuration model introduced by Bollobas [34]. All nodes are initially assigned a fixed degree $d_i = k, i \in \mathcal{N}$. The k degree stubs are then randomly interconnected while avoiding self-loops and multiple links.

- **Barabási-Albert (BA)**: growth model proposed by Barabási *et. al.* [1] whereby new nodes are attached to m already existing nodes in a preferential attachment fashion. For large enough values of N, this method ensures the emergence of *power-law* behavior observed in many real-world networks.

- **Watts-Strogatz (WS)**: randomized circular lattice proposed by Watts *et. al.* [2] where all nodes start with a fixed degree k and are connected to their $\frac{k}{2}$ immediate

neighbors. In a second stage, all existing links are rewired with a small probability p, which produces graphs with low average hopcount yet high clustering coefficient, which mimics the *small-world* property found in real-world networks.

- **Lattice (LA)**: a deterministic three-dimensional grid which loops around its boundaries (i.e. a geometrical torus).

These models exhibit a wide variety of topological features and represent the four different building blocks of A_1 and A_2. The input parameters for each model are set such that all graphs have the same number of nodes and links. In addition, all simulated graphs consist of a single connected component, i.e. random graphs containing more than one connected component were discarded.

In addition to the four model networks, we define two quenched strategies to generate the interdependency matrix B

- *diagonal interlinking* strategy: links are randomly added to the diagonal elements of B, thus linking single network's analogous nodes.

- *random interlinking* strategy: random links are uniformly added to B without restrictions, generating a random interconnection pattern.

In Section 3.1 we analytically solved the annealed counterparts, which prove to be accurate approximations for the proposed interlinking strategies.

In the next sections, we explore the effects of the two interlinking strategies on the Fiedler partition of our interdependent model, which are testimony of the phase transition experienced by μ_{N-1}.

4.2. Diagonal Interlinking Strategy

4.2.1. Initial and final states

We will refer to the *natural*, *initial* or *unperturbed* state as the scenario where there exist no interlink connecting the two networks G_1 and G_2. In this scenario, the algebraic connectivity dips to a null value due to the networks being disconnected [26]; the Fiedler partition then becomes undetermined. Nevertheless, the sign of the $x^{(0)}$ components allows splitting the network into two clusters $\mathcal{P} = G_1$ and $\mathcal{Q} = G_2$, corresponding to the two unperturbed networks.

The *final* state of the diagonal interlink strategy corresponds to N_1 added interlinks, thus $B = I$ and the Fiedler vector becomes the vector $(x(Q_1), x(Q_1))$, as proved in section 3.1. Therefore, the final partition depends exclusively on G_1 and G_2, independently of B. Assuming that both networks are equal $G_1 = G_2$, the final cut consists of a subset of intralinks of A_1, as illustrated in Fig. 1c. The critical point for the diagonal strategy is characterized by a transition from an interlink cut to an intralink cut as illustrated in Fig. 3. The transition takes place after adding a set number of links, beyond which $\mu(Q)$ remains constant. In other words, a phase transition occurs when the algebraic connectivity of the interdependent network $\mu(Q)$ reaches the algebraic connectivity of the single networks $\mu(Q_1)$.

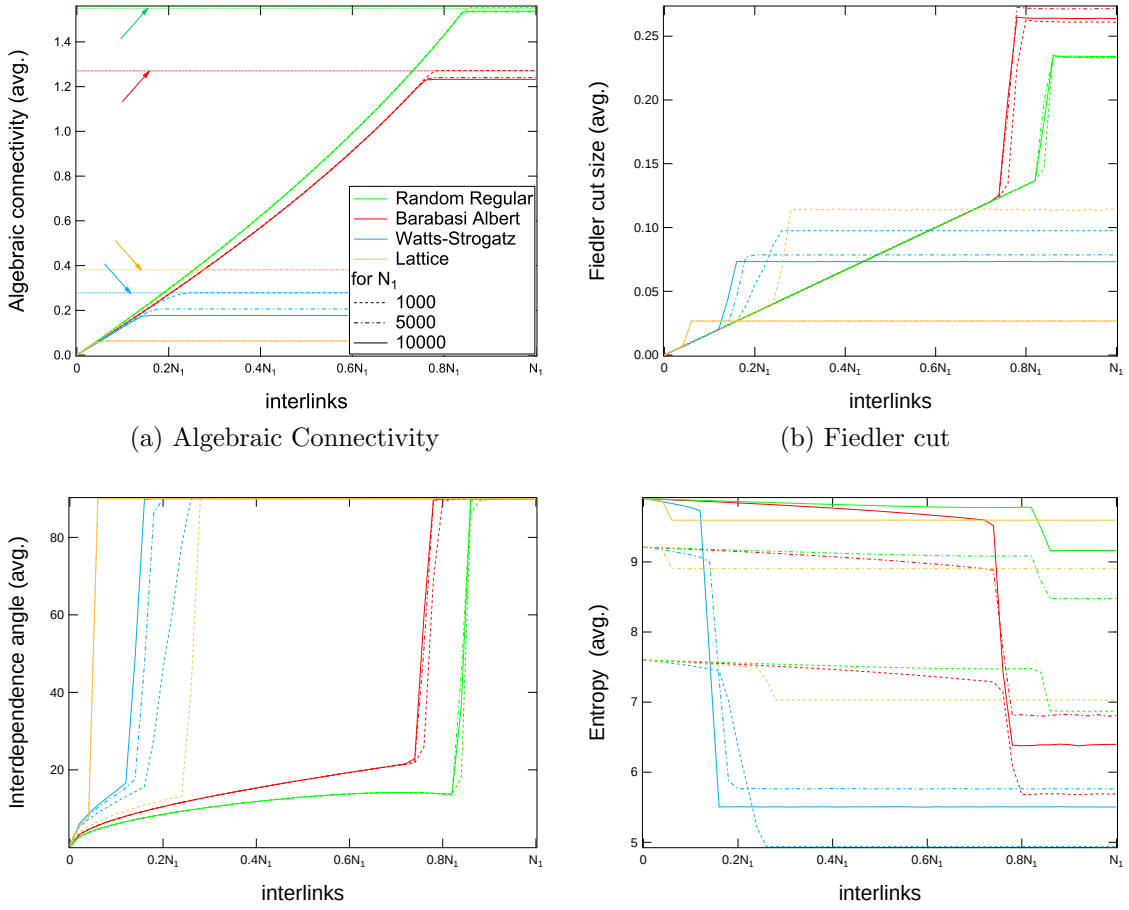

(a) Algebraic Connectivity

(b) Fiedler cut

(c) Interdependence angle

(d) Entropy

Figure 4: (Color online) Four metrics' averages are displayed to evaluate the effect of adding interlinks following the diagonal strategy: algebraic connectivity (μ), Fiedler cut ($l(\mathcal{R},\mathcal{S})/L_1+L_2$), interdependence angle ($acos\left(x^T x^{(0)}/\left\|x\right\|\left\|x^{(0)}\right\|\right)$), and entropy ($-\sum_{i=1}^{N} {x_i}^2 \log {x_i}^2$). All metrics experience a transition that sharpens for increasing N. BA and RR graphs transition around 80% added interlinks, whereas WS and LA graphs transition around 20%. The size of the network N_1 has a relatively little impact on BA and RR curves, which suggests that the transition is independent of the network size N_1. The flat lines signaled with arrows in the top left plot benchmark the average algebraic connectivity of the $N_1 = 1,000$ respective single networks.

This transitional effect is clearly visible from the spectral partitioning metrics displayed in Fig. 4; Fig. 5. shows how the transitional region narrows upon increasing N, as it approaches an asymptotic value. Our mean field theory predicts this critical value to be $l_I = \frac{\mu(Q_1)\cdot N_1}{2}$, as exposed in section 3.1.

The precise location of the jump in the simulated experiment, i.e. the critical value of interlinks per node l_I, depends on the graph model. Regardless, the phase transition is a general phenomenon, which occurrence only depends on the fact that there exists a Fiedler cut for the single networks.

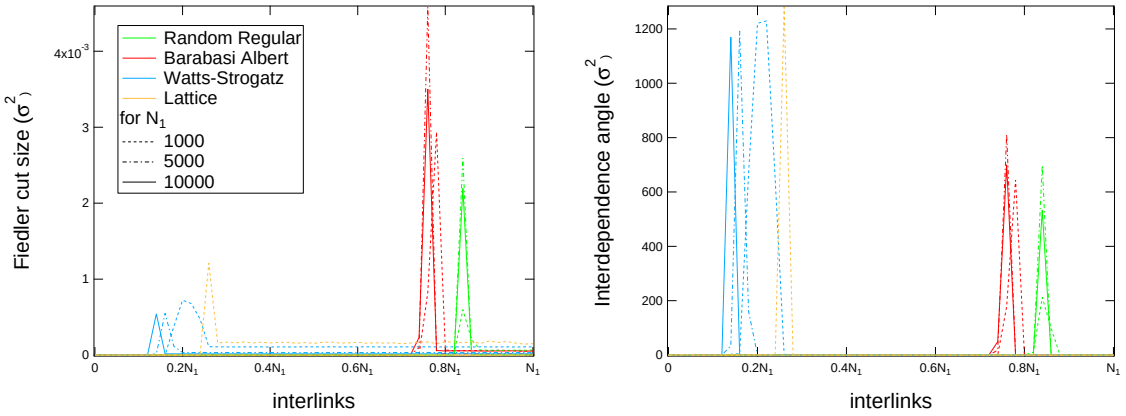

(a) Fiedler cut (b) Interdependence angle

Figure 5: (Color online) The fluctuation σ^2 of the Fiedler cut and the interdependence angle are displayed to evaluate the effect of adding interlinks following the diagonal strategy. The narrowing peaks illustrate the sharpening of the transition observed in Fig. 4. The narrowing effect is specially noticeable in the Watts-Strogatz model (blue curves).

4.2.2. Spectral partitioning metrics

We further investigate the properties of the phase transition, by looking at how the partition metrics displayed Fig. 4 evolve as interlinks are added to the B matrix.

The algebraic connectivity (Fig. 4a) starts at its minimum value $\approx \frac{1}{2N_1}$ as predicted, which increases almost linearly until it reaches its maximum value $\mu(Q_1)$ when sufficient interlinks are added. This means that a network with 100% diagonal interlinks and the same network with 90% interlinks synchronize virtually at the same speed. Comparing the final values of the algebraic connectivity, it is remarkable that random networks synchronize faster than lattice networks. This is reasonably due to the longer average distance in the latter.

The Fiedler cut (Fig. 4b) starts at $\frac{1}{2L_1}$ for a single added interlink. Notice that it increases linearly with the percentage of interlinks, because all added interlinks directly become part of the Fiedler cut. For all networks, we observe a tipping point (which depends on the network type) upon which adding a single link abruptly readjusts the partition: the Fiedler cut switches from pure interlink cutting to a cutting of an invariable set of intralinks.

The interdependence angle (Fig. 4c) tells us that the Fiedler vector starts being parallel to the first order approximation $x^{(0)}$ for 1 added interlink. Progressively, the Fiedler vector crawls the N-dimensional space up to the transition point, where it abruptly jumps to the final (orthogonal) state $(x(Q_1), x(Q_1))$. Similarly to the interdependence angle, the high values of entropy (Fig. 4c) reflect the flatness of $x^{(0)}$, where all components have (almost) the same absolute value. At this initial point, entropy is maximum and almost equal to $log(2N_1)$, which tells us that the initial partition consists purely of interlinks. When the partition turns to the final state, the entropy is instantly shaped by the network topologies of A_1 thus dropping to relatively much lower values. Notice that, for all values of N, the

highest final entropy is attained by the lattice graph due to its homogeneous structure, as seen in Fig. 4.

4.3. Random Interlinking Strategy

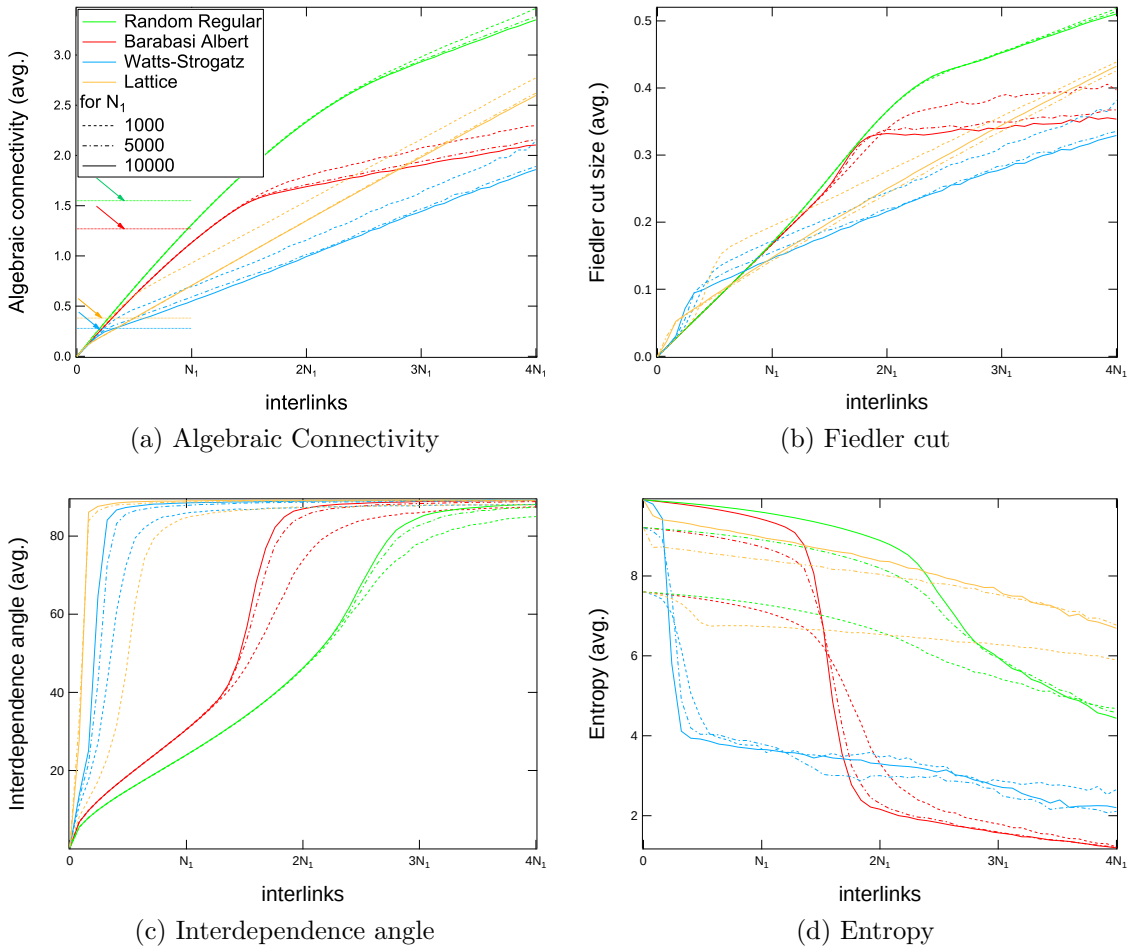

(a) Algebraic Connectivity

(b) Fiedler cut

(c) Interdependence angle

(d) Entropy

Figure 6: (Color online) Four metrics' averages are displayed to qualitatively evaluate the effect of adding interlinks following the random strategy: algebraic connectivity (μ), Fiedler cut ($l(\mathcal{R},\mathcal{S})/L_1 + L_2$), interdependence angle ($acos\left(x^T x^{(0)}/\left\|x\right\|\left\|x^{(0)}\right\|\right)$), and entropy ($-\sum_{i=1}^{N} {x_i}^2 \log {x_i}^2$). The four metrics indicate the existence of up to three regimes, but the regime transitions are not as sharp as in the diagonal strategy scenario. The flat lines signaled with arrows in the top left plot represent the average algebraic connectivity of the $N_1 = 1,000$ respective single networks.

Upon the progressive addition of random interlinks, the algebraic connectivity of all models experiences two regimes, as observed in Fig. 6a. Initially, for a weak coupling, the algebraic connectivity reaches a minimum as is the case for the diagonal strategy and represents a good starting point for the perturbation theory. If we slightly increase the number of interlinks, the average algebraic connectivity and Fiedler cut curves show a linear increase. When we reach the critical number of links $l_J = \mu \cdot N$, the algebraic connectivity μ

swaps with μ_{N-2}, causing the slope to decrease by a factor of two, as can be seen from Fig.6a and Fig. 6b. These observations are in perfect agreement with our theoretical prediction (10). However, additional simulations revealed that not only the average, but also the fluctuations steadily increase in the same fashion as in Fig. 5, which is expected due to the large set of available graph configurations.

As we can see from the interdependence angle in Fig. 6c, in the first regime the natural partition is partially preserved up to l_J. At this turning point, the interdependence angle experiences a sharp increase. This is due to the fact that the Fiedler cut in all our isolated model networks scales less than linearly with the network size, which is consistent with the picture of a phase transition between a Fiedler cut dominated by interlinks. As opposed to the diagonal strategy, the final eigenvector of the random strategy is not strictly identical to the Fiedler eigenvector of the isolated networks x, but it also involves interlink cuts. This is due to the fact that in the general case x does not belong to the kernel of Q_B, as opposed to the diagonal case.

The exact location of the phase transition can also be predicted employing perturbation theory, by imposing the perturbed value $x(Q)$ of the configuration to be equal to that achieved starting from the $x(Q_1)$ initial state. However, the resulting formulas are not particularly simple and their numerical calculation requires a time comparable with the Fiedler eigenvalue evaluation of the sparse metrics. For this reasons such estimates are not reported here.

4.4. Network Model Differences

In this section we briefly discuss the differences that arise between the four network models. For the diagonal strategy, we observed that RR and BA synchronize relatively faster than deterministic networks. This is due to random interconnections shortening the average hopcount, thus the so called *small-world* effect [2]) is exhibited. For the particular case of BA, we observe the emergence of a dominant partition which contains approximately 90% of the total number of nodes.

The difference between random and grid networks still exists for the random strategy, but it is not as dominant as in the diagonal case. This effect is expected due to the randomization resulting from the random addition of links to regular structures, which is the conceptual basis of the WS model. In general, we observe that the optimal link addition strategy depends on the network topology.

We observe from Fig. 6a that the random strategy synchronizes more slowly than that of RR and BA. On the other hand, the random strategy synchronizes faster in WS and LA models. Thus if we were to add precisely N_1 random interlinks between two identical networks, regular structures benefit more than random ones.

To test whether the phase transition is merely an artifact of our synthetic models, additional simulations were carried out using real topologies from a public dataset. Simulation results verify that the transition from the natural partition to the final orthogonal partition also occurs in real networks in the Koblenz Network Collection. The transition in real networks takes place very early in the link addition process, due to the poor synchronization capabilities of networks not designed for such purpose. The positive interpretation of such

result is that, to provide a real network with a complete backup mirror without adding diffusive delays, a small number of interlinks are required.

5. Conclusions

Our contribution beacons a significant starting point to the understanding of diffusion driven dynamics on interdependent networks. Having in mind synchronization applications, this work focuses on the algebraic connectivity of interdependent networks. We provided evidence that upon increasing the number of interlinks between two originally isolated networks, the algebraic connectivity experiences a phase transition. That is, there exists a critical number of *diagonal interlinks* beyond which any further inclusion does not enhance the algebraic connectivity μ_{N-1} at all. Similarly, there exists a critical number of *random interlinks* beyond which algebraic connectivity increments at half of the original rate.

We have observed that the phase transition is a generalized phenomena, which occurrence is independent of the graph models at hand. However, the precise number of links that triggers the critical transition does depend on the topology of the graph models. In particular, we observed that the transition point shifts almost linearly with the μ_{N-1} of the single nets, and since μ_{N-1} is monotonous with assortativity [35, 36], the transition point also increases with assortativity. We have performed additional simulations for networks with increasing assortativity, which confirm our prediction. We analytically derived the critical transition threshold for both, the diagonal and random interlinking strategies, by mean field approximations. The transitions occur upon adding: $\frac{\mu(Q_1)\cdot N_1}{2}$ links for the *diagonal interlinks* strategy, and $\mu(Q_1)\cdot N_1$ links for the *random interlinking* strategy. Moreover, we show that the critical number of interlinks that trigger the transition can also be estimated looking at the homogeneity of the NoN's spectra, i.e. the entropy of the Fiedler vector.

Preliminary results show that heterogeneous interdependent networks do also experience the same type of transition; analysis of this general case are subject of ongoing work. Other extensions could encompass additional graph models and broader collections of interlinking strategies.

Acknowledgements

This research has been partly supported by the European project MOTIA (Grant JLS-2009-CIPS-AG-C1-016); the EU Research Framework Programme 7 via the CONGAS project (Grant FP7-ICT 317672); and the EU Network of Excellence EINS (Grant FP7-ICT 288021).

[1] A. L. Barabasi, R. Albert, Emergence of scaling in random networks, Science 286 (5439) (1999) 509–512.
[2] D. J. Watts, S. H. Strogatz, Collective dynamics of small world networks, Nature 393 (1998) 440–442.
[3] P. Van Mieghem, The N-intertwined SIS epidemic network model, Computing 93 (2-4) (2011) 147–169.
[4] A. Bergen, D. Hill, A structure preserving model for power system stability analysis, Power Apparatus and Systems, IEEE Transactions on PAS-100 (1) (1981) 25 –35.
[5] M. Barahona, L. M. Pecora, Synchronization in small-world systems, Phys. Rev. Lett. 89 (2002) 054101. doi:10.1103/PhysRevLett.89.054101.
[6] F. M. Atay, T. Biyikoglu, J. Juergen, Synchronization of networks with prescribed degree distributions, IEEE Transactions on Circuits and Systems-I 53 (1) (2006) 92–98.

[7] J. Chen, J. Lu, C. Zhan, G. Chen, Laplacian Spectra and Synchronization Processes on Complex Networks, Springer Optimization and Its Applications, 2012, Ch. 4, pp. 81–113.
[8] F. B. Florian Dörfler, Exploring synchronization in complex oscillator networks, Synchronization tutorial paper for 51st IEEE Conference on Decision and Control (CDC).
[9] X. F. Wang, G. Chen, Synchronization in scale-free dynamical networks: robustness and fragility, Circuits and Systems I: Fundamental Theory and Applications, IEEE Transactions on 49 (1) (2002) 54 –62.
[10] S. Strogatz, From kuramoto to crawford: Exploring the onset of synchronization in populations of coupled oscillators., Physica D 143 (2000) 1–20.
[11] L. M. Pecora, T. L. Carroll, Master stability functions for synchronized coupled systems, Phys. Rev. Lett. 80 (1998) 2109–2112. doi:10.1103/PhysRevLett.80.2109.
[12] A. Jadbabaie, N. Motee, M. Barahona, On the Stability of the Kuramoto Model of Coupled Nonlinear Oscillators, in: In Proceedings of the American Control Conference, 2004, pp. 4296–4301.
[13] J. A. Acebrón, L. L. Bonilla, C. J. Pérez-Vicente, F. Ritort, R. Spigler, The Kuramoto model: A simple paradigm for synchronization phenomena, Rev. Mod. Phys. 77 (2005) 137–185.
[14] R. Olfati-Saber, Ultrafast consensus in small-world networks, in: Proceedings of the American Control Conference, IEEE, Los Alamitos, CA, USA, 2005, pp. 2371–2378.
[15] R. Freeman, P. Yang, K. Lynch, Distributed estimation and control of swarm formation statistics, in: American Control Conference, 2006, 2006, pp. 7 pp.–. doi:10.1109/ACC.2006.1655446.
[16] A. Jamakovic, S. Uhlig, On the relationship between the algebraic connectivity and graph's robustness to node and link failures, in: Next Generation Internet Networks, 3rd EuroNGI Conference on, Trondheim, Norway, 2007, p. 96.
[17] M. Fiedler, A property of eigenvectors of nonnegative symmetric matrices and its application to graph theory, Czechoslovak Mathematical Journal 25.
[18] S. H. Strogatz, Exploring complex networks, Nature 410 (6825) (2001) 268–276. doi:10.1038/35065725.
[19] T. Yamamoto, H. Sato, A. Namatame, Evolutionary optimised consensus and synchronisation networks, IJBIC 3 (3) (2011) 187–197.
[20] Simpson-Porco, J. W. Dorfler, B. F. Florian, Droop-controlled inverters are kuramoto oscillators, in: IFAP Workshop on Distributed Estimation and Control of Networked Systems, Vol. 3, 2012, pp. 264–269.
[21] R. Olfati-Saber, H. Dartmouth Coll., Algebraic connectivity ratio of ramanujan graphs, in: American Control Conference, 2007, pp. 4619 – 4624.
[22] A. Arenas, A. Diaz-Guilera, J. Kurths, Y. Moreno, C. Zhou, Synchronization in complex networks, Physics Reports 469 (2008) 93–153.
[23] Y. Shang, Synchronization in networks of coupled harmonic oscillators with stochastic perturbation and time delays, Mathematics and its Applications : Annals of the Academy of Romanian Scientists 4 (1) (2012) 44.
[24] P. Lin, Y. Jia, Average consensus in networks of multi-agents with both switching topology and coupling time-delay, Physica A: Statistical Mechanics and its Applications 387 (1) (2008) 303 – 313.
[25] L. Donetti, F. Neri, M. A. Munoz, Optimal network topologies: Expanders, Cages, Ramanujan graphs, Entangled networks and all that, Journal of Statistical Mechanics: Theory and Experiment 8.
[26] P. Van Mieghem, Graph Spectra for Complex Networks, Cambridge University Press, 2010.
[27] H. Wang, Q. Li, G. D'Agostino, S. Havlin, H. E. Stanley, P. Van Mieghem, Effect of the interconnected network structure on the epidemic threshold, Phys. Rev. E 88 (2013) 022801.
[28] S. V. Buldyrev, R. Parshani, G. Paul, H. E. Stanley, S. Havlin, Catastrophic cascade of failures in interdependent networks, Nature 464 (7291) (2010) 1025–1028.
[29] E. A. Leicht, M. D. Raissa, Percolation on interacting networks, arXiv:0907.0894.
[30] S. Gómez, A. Díaz-Guilera, J. Gómez-Gardeñes, C. J. Pérez-Vicente, Y. Moreno, A. Arenas, Diffusion dynamics on multiplex networks, Phys. Rev. Lett. 110 (2013) 028701. doi:10.1103/PhysRevLett.110.028701.
[31] M. Fiedler, Algebraic connectivity of graphs, Czechoslovak Math 23/98 (1973) 298–305.

[32] J. Wilkinson, The Algebraic Eigenvalue Problem, Oxford University Press, New York, 1965.
[33] S. J. Blundell, K. M. Blundell, Concepts in thermal physics, Oxford University Press, 2010.
[34] B. Bollobas, Random Graphs, 2nd Edition, Cambridge University Press, Cambridge, 2001.
[35] G. D'Agostino, A. Scala, V. Zlatić, G. Caldarelli, Robustness and assortativity for diffusion-like processes in scale-free networks, Europhysics Letters 97 (6) (2012) 68006.
[36] D. Zhou, E. Stanley, G. DAgostino, A. Scala, Assortativity decreases the robustness of interdependent networks, Physical Review E 86 (6) (2012) 066103.

Appendix A. Approximating μ using perturbation theory

We want to find the minimum that satisfies the spectral equations:

$$\begin{cases} (Q_A + \alpha Q_B - \mu I)x &= 0, \\ x^T x &= 1, \\ u^T x &= 0. \end{cases} \tag{A.1}$$

When the solution is analytical in α, one may express μ and x by Taylor expansion as

$$\mu = \sum_{k=0}^{\infty} \mu^{(k)} \alpha^k \tag{A.2}$$

$$x = \sum_{k=0}^{\infty} x^{(k)} \alpha^k \tag{A.3}$$

Substituting the expansion in the eigenvalue equation (13) gives the hierarchy of equations:

$$\begin{cases} Q_A x^{(k)} + \alpha Q_B x^{(k-1)} &= \sum_{i=0}^{k} \mu^{(k-i)} x^{(i)} & \textit{for all } k, \\ \sum_{i=0}^{k} x^{(k-i)} x^{(i)} &= 0 & \textit{for } k \geq 1, \\ u^T x^{(k)} &= 0 & \textit{for all } k. \end{cases} \tag{A.4}$$

Appendix A.1. Explicit approximations up to the second order

The zero order expansion of (A.4) provides a simple set of equations:

$$\begin{cases} Q_A x^{(0)} &= \mu^{(0)} x^{(0)}, \\ x^{(0)} x^{(0)} &= 1, \\ u^T x^{(0)} &= 0. \end{cases} \tag{A.5}$$

Let $(\mu_{N-1})_{A1}, (\mu_{N-1})_{A2}$ and $(x_{N-1})_{A1}, (x_{N-1})_{A2}$ denote the smallest non-zero eigenvalue and the corresponding eigenvector of Q_1, Q_2, respectively. Similarly

$$\begin{cases} (x_{N_1})_{A1} &= 1/\sqrt{N_1}(1, 1, \ldots, 1, 0, 0, \ldots, 0), \\ (x_{N_2})_{A2} &= 1/\sqrt{N_2}(0, 0, \ldots, 0, 1, 1, \ldots, 1). \end{cases} \tag{A.6}$$

will represent the null eigenvectors of network G_1 and G_2, respectively. When the networks are put together, any combination of the former is a null eigenvector. Two special combinations are worth employing: the trivial solution corresponding to the constant vector:

$$x_N = \frac{1}{\sqrt{N}}(1,\ldots,1) = \sqrt{\frac{N_1}{N}}(x_{N_1})_{A1} + \sqrt{\frac{N_2}{N}}(x_{N_2})_{A2}. \tag{A.7}$$

and the other combination orthogonal to the former that represents a useful starting point for the perturbation theory:

$$x^{(0)}_{N-1} = x^{(0)} = \frac{1}{\sqrt{N}}(1,\ldots,1,-1,\ldots,-1) = \sqrt{\frac{N_1}{N}}(x_{N_1})_{A1} - \sqrt{\frac{N_2}{N}}(x_{N_2})_{A2}. \tag{A.8}$$

which satisfies the zero order approximation (A.5). The zero order approximation to the Fiedler eigenvalue is then null:

$$\mu^{(0)} = 0. \tag{A.9}$$

The first order approximation equations follow from (A.4) as:

$$\begin{cases} Q_A x^{(1)} + \alpha Q_B x^{(0)} &= \mu^{(1)} x^{(0)} \\ \left(x^{(0)}\right)^T x^{(1)} &= 0 \\ u^T x^{(1)} &= 0. \end{cases} \tag{A.10}$$

Taking the projection over $x^{(0)}$ of the first equation of (A.10), one obtains the first order correction $\mu^{(1)}$ that depends on the zero order eigenvector only:

$$\mu^{(1)} = \left(x^{(0)}\right)^T \alpha Q_B x^{(0)} \tag{A.11}$$

A simple case to analyze is that where only one interlink joins A_1 with A_2: $(B_{12})_{ij} = \delta_{ik}\delta_{kj}$; in this case $(d_1)_{kk} = \delta_{ik}$ and $(d_2)_{ll} = \delta_{jl}$ and the perturbation estimate gives:

$$\mu^{(1)} = (\frac{1}{2}(1+1)+1)(\eta_i)^2 = \frac{2}{N_1} \geq \mu_{N-1}(Q). \tag{A.12}$$

where η is the single net (N_1 dimensional) unitary vector $\eta \stackrel{def}{=} 1/\sqrt{N_1}(1,1,\ldots,1)$. When k interlinks are included, Q_B is just the sum of k contributions of the previous type thus $\mu^{(1)} = \frac{2k}{N_1}$. That is, the first order correction to the Fiedler eigenvalue increases linearly with the number of interlinks. The first order correction to the eigenvector can be evaluated from (A.10) as a solution of the linear equation:

$$Q_A x^{(1)} = -\left(Q_B - \mu^{(1)}\right) x^{(0)}. \tag{A.13}$$

where the operator Q_A is invertible out of its kernel ($Q_A v = 0$); since $\left(\alpha Q_B - \mu^{(1)}\right) x^{(0)}$ is orthogonal to the kernel, (A.13) is solvable.

The second order equations follow from (A.4) as

$$\begin{cases} Q_A x^{(2)} + \alpha Q_B x^{(1)} &= \mu^{(0)} x^{(2)} + \mu^{(1)} x^{(1)} + \mu^{(2)} x^{(0)} \\ \left(x^{(0)}\right)^T x^{(2)} + \left(x^{(1)}\right)^T x^{(1)} + \left(x^{(2)}\right)^T x^{(0)} &= 0 \\ u x^{(2)} &= 0 \end{cases} \tag{A.14}$$

that is, the second order correction is quadratic and equals:

$$\mu^{(2)} = \left(x^{(0)}\right)^T Q_B \left(x^{(1)}\right) = -\left(x^{(1)}\right)^T Q_A \left(x^{(1)}\right) \leq 0. \tag{A.15}$$

As expected $\mu^{(2)}$ is negative, thus improving the estimate of the algebraic connectivity. The former perturbation estimates are illustrated in Fig. 3 together with numerical simulations.

Perturbation theory may also be applied to any initial eigenvector of the unperturbed networks. Different perturbations αB will have different effects on the quadratic form of (13) associated with all initial eigenvectors. Therefore, it may happen that the perturbed value of μ obtained starting from $x^{(0)}$ is smaller than the quadratic form associated with the x_{N-1} (the unperturbed eigenvector in (6)) or some other educated guess. This is precisely the origin of the phase transition.

The estimates resulting form the second order perturbation theory are compared in Fig. 3 with the results of numerical calculations. As can be seen, for both the diagonal and the random strategies the agreement is good up to the phase transition where the starting point of the perturbation theory should be changed.

Appendix A.2. Perturbative approximations and exact upper bounds

Since we are dealing with a constraint optimization problem, finding a minimum of a positive form, any test vector v provides an upper bound for the actual minimum value:

$$\mu = \mu_{N-1} \leq \frac{v^T Q v}{v^T v}. \tag{A.16}$$

The perturbation theory provides natural candidates as test vectors. The zero order solution provides the simplest inequality:

$$\mu_{N-1}(Q) \leq \alpha \frac{(x^{(0)})^T Q x^{(0)}}{(x^{(0)})^T x^{(0)}} = \alpha \mu^{(1)}. \tag{A.17}$$

The first order approximation provides a better (i.e. lower) upper bound:

$$\mu_{N-1}(Q) \leq \frac{(x^{(0)} + \alpha x^{(1)})^T Q (x^{(0)} + \alpha x^{(1)})}{(x^{(0)} + \alpha x^{(1)})^T (x^{(0)} + \alpha x^{(1)})}.$$

that is:

$$\mu_{N-1}(Q) \leq \frac{\alpha \mu^{(1)} + \alpha^2 \mu^{(2)} + \alpha^3 (x^{(1)})^T Q_B x^{(1)}}{1 + \alpha^2 (x^{(1)})^2}. \tag{A.18}$$

which for small enough α is always lower than $\alpha \mu^{(1)}$.